Benign and Malignant Orbital Lymphoproliferative Disorders: Differentiating Using Multiparametric MRI at 3.0T

Xiao-Quan Xu, MD,[1] Hao Hu, MD,[1] Hu Liu, MD, PhD,[2] Jiang-Fen Wu, MD,[3] Peng Cao, MD,[3] Hai-Bin Shi, MD, PhD,[1]* and Fei-Yun Wu, MD, PhD[1]*

Purpose: To determine the optimal combination of parameters derived from 3T multiparametric (conventional magnetic resonance imaging [MRI], diffusion-weighted [DW] and dynamic contrast-enhanced [DCE]) MRI for differentiating malignant from benign orbital lymphoproliferative disorders (OLPDs).

Materials and Methods: Forty patients with OLPDs (18 benign and 22 malignant) underwent conventional 3.0T MR, DW, and DCE-MRI examination for presurgery evaluation. Conventional MRI features (including tumor laterality, shape, number of involved quadrants, signal intensity on T_1-weighted imaging (WI) and T_2WI, flow void sign on T_2WI, and findings suggestive of sinusitis) were reviewed, and multivariate logistic regression analysis was used to identify the most significant conventional MRI features. Apparent diffusion coefficient (ADC) and DCE-MRI derived parameters (area under curve [AUC], time to peak [TTP], maximum rise slope [Slope$_{max}$]) were measured and compared between two groups. Receiver operating characteristic (ROC) curve analyses were used to determine the diagnostic ability of each combination that was established based on identified qualitative and quantitative parameters.

Results: Multivariate logistic regression analysis showed that the presence of flow void sign on T_2WI significantly associated with benign OLPDs ($P = 0.034$). Malignant OLPDs demonstrated significantly lower ADC ($P = 0.001$) and AUC ($P = 0.002$) than benign mimics. ROC analyses indicted that, ADC alone showed the optimal sensitivity (threshold value, 0.886×10^{-3} mm^2/s; sensitivity, 90.9%), while a combination of no presence of flow void sign on T_2WI + ADC $\leq 0.886 \times 10^{-3}$ mm^2/s + AUC ≤ 7.366 showed optimal specificity (88.9%) in differentiating benign from malignant OLPDs.

Conclusion: Multiparametric MRI can help to differentiate malignant from benign OLPDs. DWI offers optimal sensitivity, while the combination of conventional MRI, DWI, and DCE-MRI offers optimal specificity.

J. MAGN. RESON. IMAGING 2016;00:000–000.

Orbital lymphoproliferative disorders (OLPDs) represent a broad spectrum of benign and malignant lesions, including lymphoid hyperplasia, atypical lymphoid hyperplasia, lymphoma, and idiopathic inflammatory pseudotumor.[1,2] Besides these, orbital IgG4-related disease (IgG4-RD) is becoming increasingly recognized and incorporated into benign OLPDs groups based on recent surveillance.[3]

In terms of treatment, orbital lymphoma is amenable to low-dose radiation therapy, whereas benign mimics usually exhibit a positive response to corticosteroid therapy.[3,4]

Therefore, preoperative differentiation of benign and malignant OLPDs has a treatment planning benefit. The clinical differentiation between these two entities is limited.[3] Therefore, there is a need for an effective method to differentiate these two entities.

Magnetic resonance imaging (MRI) plays an important role in evaluating the extent of orbital lesions, and provides supplementing information beyond clinical examination.[1,5,6] A prior study indicated that some specific imaging features such as tumor shape, presence of flow void

TABLE 1. Demographic and Histological Characteristics of OLPD Patients

Parameters	Benign OLPD Group ($n =$ 18)	Malignant OLPD Group ($n =$ 22)	P value
Mean age	50.4 ± 14.4	62.0 ± 13.6	0.022
Gender (F/M)	5 : 13	8 : 14	0.564
Histologic subtypes	IIP (8)	MALT lymphoma (17)	
	RLH (6)	DLBCL (3)	
	IgG4-related disease (4)	Follicular lymphoma (2)	

F, female; M, male; MALT, mucosa-associated lymphoid tissue; DLBCL, diffuse large B-cell lymphoma; IIP, idiopathic inflammatory pseudotumor; IgG4-RD, IgG4 related disease; RLH, reactive lymphoid hyperplasia. Data in parentheses indicate the number of the corresponding patients in our study.

sign, and imaging findings suggestive of sinusitis might be potentially useful for differentiating benign from malignant OLPDs.[3] However, the qualitative assessment of MRI features is a subjective process with limited interreader reproducibility, hence indicating a need for more objective methods to improve the diagnostic accuracy and confidence.

To date, there have been a few investigations that used functional MRI techniques to assess the orbital tumors, including diffusion-weighted (DW) and dynamic contrast-enhanced (DCE) MRI.[7–14] One previous study by Haradome et al reported that the orbital lymphoma showed significantly lower apparent diffusion coefficient (ADC) value than benign OLPDs, which might be associated with the higher cellularity in lymphoma and interstitial edematous changes in benign OLPDs.[3] Besides diffusion characteristics, angiogenesis is also an important tumor hallmark that deserves systematic assessment.[15]

DCE-MRI is an emerging imaging technique that allows quantification of various vascular biomarkers.[16] It has been reported to be useful for various applications, such as differentiating lung cancer from benign solitary pulmonary lesions, assessing the different T stage of nasopharyngeal carcinoma, noninvasively evaluating the immature mean vessel density of brain gliomas, and predicting the treatment response for patients with multiple myeloma.[16–20]

Therefore, the purpose of this study was to determine the optimal combination of parameters derived from 3T multiparametric MRI (conventional MR, DW, and DCE) for differentiating malignant from benign OLPDs.

MATERIALS AND METHODS

Patients

Our Institutional Review Board approved this retrospective study, and written informed consent was waived. A review of our hospital database identified 59 clinically or histologically confirmed OLPDs patients who underwent orbital MR examination for disease evaluation between March 2013 and January 2016.

Among these patients, 40 patients (27 men and 13 women; mean age, 57.4 ± 15.6 years; range, 22–79 years) were included in our study according to the following criteria: 1) the diameter of the lesions exceeded 1 cm; 2) no biopsy or corticosteroid therapy was administered before the MRI scan; 3) both DW and DCE-MRI were scanned; and 4) there was adequate imaging quality without obvious susceptibility artifacts.

The group pf 40 OLPDs patients was comprised of 18 benign (13 men and 5 women; mean age, 50.4 ± 14.4 years; range, 22–67 years) and 22 malignant (14 men and 8 women; mean age, 62.0 ± 13.6 years; range, 40–79 years) patients. Detailed demographic and histological information for the two groups is shown in Table 1. The final diagnosis was made based on the surgical pathological results in 35 patients, and on the follow-up after steroid treatment in five patients with presumed, inflammatory pseudotumors.

MRI

All images were acquired with a 3.0T MRI system (Verio; Siemens, Erlangen, Germany) with a 12-channel head coil. Conventional unenhanced imaging protocols contained an unenhanced axial T_1-weighted imaging (repetition time [TR] / echo time [TE], 600/10 msec), axial T_2-weighted imaging (WI) (TR/TE, 4700/79 msec) with fat saturation, and coronal T_2WI (TR/TE, 3500/79 msec).

DWI was performed in the axial plane by using a single-shot spin-echo echo-planar imaging sequence for all patients. The following imaging parameters were used: TR/TE, 4000/85 msec; section thickness, 4 mm; intersection gap, 0 mm; flip angle (FA), 150°; number of averages, 6; field of view (FOV), 200 × 200 mm; matrix, 384 × 384; and number of sections, 10. The b values used were 0 and 800 sec/mm^2. The total acquisition time of DWI was 4 minutes 14 seconds. ADC maps were automatically generated.

DCE-MRI was performed in the axial plane using a 2D turbo fast low angle shot (FLASH) sequence with an integrated parallel acquisition technique (iPAT). A standard dose of 0.1 mmol/kg of gadolinium-diethylene triamine pentaacetic acid (Magnevist; Bayer Schering Pharma, Berlin, Germany) was administered at a rate of 4 mL/s. The bolus of contrast material was followed by a 20-mL bolus of saline administered at the same injection rate. Contrast was administered after five baseline dynamics (total: 95

dynamics). The dynamic acquisition was performed with a temporal resolution of 3.3 seconds. The detailed parameters for the DCE-MRI were as follows: TR/TE, 474.66/1.43 msec; FA, 12°; average, 1; FOV, 230 mm; matrix, 128 × 128; section thickness, 4.5 mm; and number of sections, 7. The total acquisition time was 5 minutes 15 seconds. After the DCE-MRI scan, postcontrast axial, coronal, and sagittal T_1-weighted images were obtained.

Imaging Analysis

Qualitative image assessments were performed by two radiologists (Reader 1: X.X. with 6 years of experience; Reader 2: H.H. with 4 years of experience) who were blinded to the clinical information, histological results, and study design. If disagreement existed, consensus was reached by discussing the images with another radiologist (F.W. with 15 years of experience).

Our qualitative image assessment focused on the laterality, shape, number of involved quadrants, internal signal architecture, presence of flow void sign, and findings suggestive of sinusitis. The laterality was noted as either unilateral or bilateral. The shape was classified as regular or irregular. Similar to a prior study, the orbit was divided into four quadrants.[8] The number of involved quadrants was recorded as 1 or ≧2 quadrants involved.

Compared with that of the adjacent extraocular muscle, the signal intensity of the tumor on precontrast T_1- and T_2WI were classified as hypointense, isointense, and hyperintense. The presence of a signal void from a vessel within the lesions on T_2WI was defined as presence of flow void sign. Findings suggestive of sinusitis were judged according to the criterion proposed by a previous study,[3] including: 1) significant paranasal mucosal thickness (>4 mm); 2) fluid level; and 3) the presence of a retention cyst at each paranasal cavity. If bilateral lesions occurred, only the relatively larger one was assessed.

During ADC value measurements, all DWI data were converted into Digital Imaging and Communication in Medicine (DICOM) format and postprocessed offline with in-house software (FireVoxel; CAI^{2}R; New York University, NY).[21] The mean ADC value was calculated using the exponential fitting formula: ADC = $-$ ln (S$_b$/S$_0$) / b, where b represents the diffusion sensitivity coefficients, S$_b$ and S$_0$ represent the corresponding signal values of the given region-of-interest (ROI).

The DCE-MRI data were processed using a dedicated postprocessing software (Omni Kinetics; GE Healthcare, Milwaukee, WI). The time intensity curve (TIC) was obtained for each mass, and divided into persistent, plateau, and washout patterns according to a previous study.[14] For each TIC, the signal intensity (SI$_{pre}$ and SI$_{max}$) and time (T$_{pre}$, and T$_{peak}$) were derived. SI$_{pre}$ was defined as the precontrast signal intensity, and SI$_{max}$ was the signal intensity at maximal contrast enhancement. T$_{pre}$ and T$_{peak}$ were the time corresponding to the SI$_{pre}$ and SI$_{max}$. Then quantitative parameters including area under curve (AUC), time to peak (TTP), and maximum rise slope (Slope$_{max}$) were derived. AUC was defined as the area under the whole enhancement curve. TTP was defined as the time from T$_{pre}$ to T$_{peak}$. Slope$_{max}$ was calculated using the following formula: Slope$_{max}$ = (SI$_{max}$$-SI_{pre}$)/ [SI$_{pre}$ × (T$_{peak}$ $-$ T$_{pre}$)] × 100.

During the DW and DCE-MRI assessment, ROIs were also determined by the two radiologists mentioned above. ROIs (5.2 ±

3.1 cm^3) were placed on all imaging sections and encompassed as much as tumor area, excluding the large necrotic, cystic, and hemorrhagic areas and surrounding blood vessels referred to T_2WI and contrast-enhanced T_1WI. To minimize the effect of partial volume averaging, the edges of lesions were avoided during ROI placement. If bilateral lesions were seen, only the relatively larger lesion was included for analysis.

The quantitative assessment results of the two readers were used to evaluate the interreader reproducibility. Additionally, to evaluate intrareader reproducibility, the MRI data were quantitatively assessed again by Reader 1, with a minimum washout period of at least 1 month. The average of the two measurement results of Reader 1 was used for the statistical analysis.

Statistical Analysis

Quantitative results are expressed as mean ± standard deviation, and we used the Kolmogorov–Smirnov test for normally distributed analysis.

Univariate analysis was first performed in an attempt to characterize the ability of each variable for predicting malignant OLPDs. The frequency distribution of gender and each qualitative MRI feature between the two groups was compared with Fisher's exact test. The differences in age between the two groups were compared with an unpaired t-test. Then multivariate logistic regression analysis was used to identify the most valuable variables that were predictive of OLPDs.

The differences of mean ADC value and DCE-MRI-derived parameters between the two groups were compared using an unpaired t-test. Based on the identified qualitative MRI variables and functional MRI parameters, we established different diagnostic models. The receiver operating characteristic (ROC) curve was performed to determine the value of each diagnostic model in differentiating benign from malignant OLPDs. Sensitivity and specificity were calculated with a threshold criterion determined as the value would maximize the Youden index.

The interreader reproducibility for the conventional MRI features assessment was evaluated using kappa analysis. The inter- and intrareader reproducibility for DW and DCE-MRI parameters measurement was evaluated using the intraclass correlation coefficient (ICC) with 95% confidence intervals (CI) and applying a two-way ICC with a random rater assumption. The ICC and kappa value ranges 0–1.00, with values closer to 1.00 representing better reproducibility. They were interpreted as follows: (<0.40, poor; 0.41–0.60, moderate; 0.61–0.80, good; and ≥0.81, excellent). All statistical analyses were performed with statistical software (SPSS, v. 19.0, Chicago, IL; MedCalc, v. 9.0, MedCalc Software, Mariakerke, Belgium). The statistical significance threshold was set at a two-sided P value below 0.05, while at a P value below 0.017 (0.05/3) for the Bonferroni correction for comparison of the DCE-MRI parameters.

RESULTS

There was a significant difference in the age ($P = 0.022$), while no difference in the gender distribution ($P = 0.564$) of patients between benign and malignant OLPDs groups.

TABLE 2. Conventional MR Imaging Features of Benign And Malignant OLPDs Patients

Parameters	Benign OLPD Group ($n=18$)	Malignant OLPD Group ($n=22$)	P value	K value
Laterality			0.641	0.977
Unilateral	11	15		
Bilateral	7	7		
Shape			0.225	0.803
Irregular	8	14		
Regular	10	8		
Number of involved quadrants			0.266	0.719
1	5	3		
$\geqq 2$	13	19		
Signal intensity on T1WI			0.673	0.721
Low	17	20		
Iso	1	2		
Signal intensity on T2WI			0.781	0.758
Low	1	2		
Iso	13	15		
High	4	5		
Presence of flow void sign on T2WI			0.003	0.833
Yes	16	9		
No	2	13		
Finding suggestive of sinusitis			0.009	0.862
Yes	14	8		
No	4	14		

The signal intensity on T1- and T2-weighted imaging was compared with that of extraocular muscle.

Table 2 summarizes the frequency distribution of conventional MRI features of OLPDs patients. There were differences in the presence of flow void sign on T_2WI ($P=0.003$) and findings suggestive of sinusitis ($P=0.009$), while no significant difference in tumor laterality ($P=0.641$), shape ($P=0.225$), number of involved quadrants ($P=0.266$), signal intensity on T_1WI ($P=0.673$), or signal intensity on T_2WI ($P=0.781$) was seen between benign and malignant OLPDs groups.

Then age, presence of flow void sign on T_2WI, and findings suggestive of sinusitis were adapted into multivariate logistic regression analysis. As a result, no presence of flow void sign on T_2WI was identified as the most important qualitative imaging feature that was indicative of malignant OLPDs. Detailed multivariate logistic regression analysis results are summarized in Table 3. Setting no presence of flow void sign on T_2WI as the diagnostic criterion for malignant OLPDs, we could achieve

an AUC of 0.707, sensitivity of 63.6%, and specificity of 77.8%.

Table 4 summarizes the detailed comparisons of mean ADC value and DCE-MRI-derived parameters between the two groups. A significantly lower mean ADC value was found in malignant OLPDs compared with benign mimics ($P=0.001$) (Fig. 1a). Regarding the TIC pattern, benign OLPDs demonstrated a persistent pattern ($n=15$) or plateau pattern ($n=3$), while malignant OLPDs demonstrated a washout pattern ($n=17$) or plateau pattern ($n=5$) (Table 4). As to the DCE-MRI-derived parameters, malignant OLPDs showed lower AUC ($P=0.002$) values than benign mimics, while no significant differences were found on TTP ($P=0.026$) and Slope$_{max}$ ($P=0.327$) (Fig. 1b–d). The ROC curve results indicated that, setting AUC ≤ 7.366 as the cutoff value, the best diagnostic ability could be achieved (AUC, 0.795; sensitivity, 77.3%; specificity, 72.2%). When ADC $\leq 0.886 \times 10^{-3}$ mm^2/s was set as the

TABLE 3. Multivariate Logistic Regression Results Using Conventional MRI Features to Differentiate Benign From Malignant OLPDs

Parameters	β Coefficient	SE	Odds ratio (95%CI)	P value
Age	0.058	0.033	1.059 (0.994-1.129)	0.077
No presence of flow void sign on T2WI	−1.992	0.942	0.136 (0.022-0.865)	0.034
No finding suggestive of sinusitis	−1.250	0.837	0.287 (0.056-1.479)	0.136
SE, standard error; CI, confidence interval.				

threshold value, the best diagnostic ability could be achieved (AUC, 0.779; sensitivity, 90.9%; specificity, 61.1%).

Based on no presence of flow void sign on T_2WI, AUC ≤7.366 and ADC ≤0.886 × 10^{-3} mm^2/s, we established seven potential diagnostic combinations. ROC curves analyses results indicated that a combination of no presence of flow void sign on T_2WI + ADC ≤0.886 × 10^{-3} mm^2/s + AUC ≤7.366 showed the optimal specificity (88.9%) (Fig. 2a), while the ADC value alone showed the optimal sensitivity (90.9%) in predicting orbital malignant OLPDs (Fig. 2b). Detailed diagnostic performances of each noted parameter and diagnostic combination are summarized in Table 5. Figures 3 and 4 show the multiparametric MR images of the representative patients with orbital mucosa-associated lymphoid tissue lymphoma and idiopathic inflammatory pseudotumor.

Good or excellent interreader agreements were achieved during the qualitative assessment of conventional MRI features, while excellent inter- and intrareader agreements were achieved during the measurement of ADC and DCE-MRI derived quantitative parameters. Detailed kappa values for qualitatively assessing the conventional MRI features are listed in Table 2, and detailed ICCs for the measurement of ADC and DCE MR derived imaging parameters are listed in Table 4.

DISCUSSION

Our study found that flow void sign on T_2WI was the most significant qualitative conventional MRI feature that may be helpful in differentiating malignant OLPDs from benign mimics. With the addition of DW and DCE-MRI, optimal specificity could be achieved in the differentiation of benign and malignant OLPDs, while optimal sensitivity could be obtained in differentiating these two entities when DWI was used alone.

TABLE 4. Differences of DW and DCE-MRI-Derived Parameters Between Benign and Malignant OLPD Groups

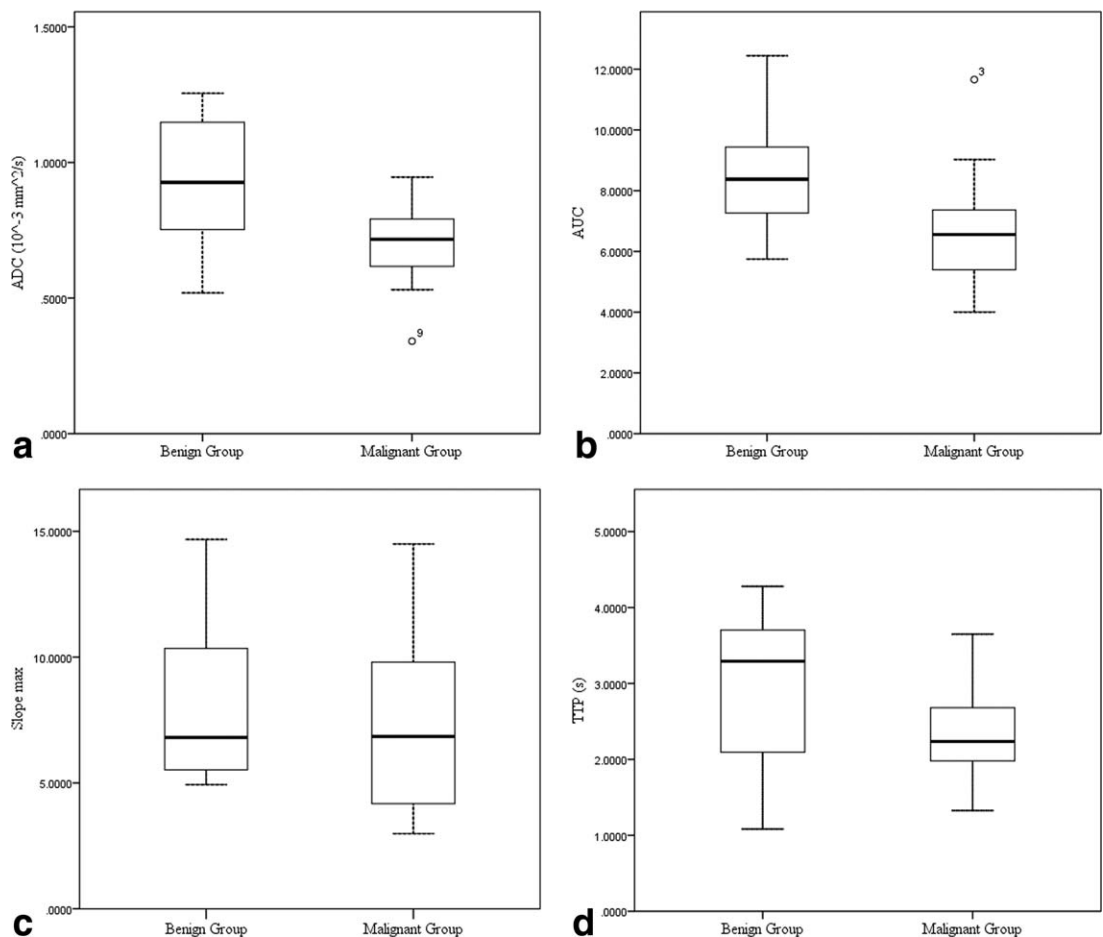| Parameters	Benign OLPD Group ($n =$ 18)	Malignant OLPD Group ($n =$ 22)	P value	ICC	
				Inter	Intra
DWI					
ADC$_{mean}$	0.927 ± 0.225	0.711 ± 0.152	0.001	0.886	0.902
DCE-MRI					
TIC pattern			–	–	–
Persistent	15	–			
Plateau	3	5			
Washout	–	17			
TTP	2.958 ± 1.047	2.340 ± 0.617	0.026	0.851	0.883
AUC	8.520 ± 1.820	6.662 ± 1.774	0.002	0.849	0.872
Slope$_{max}$	8.321 ± 3.279	7.307 ± 3.159	0.327	0.855	0.891
Except for the P values, data are reported as mean ± standard deviation. Unit for ADC value is × 10^{-3} mm^2/s. ADC, apparent diffusion coefficient; ADC$_{mean}$, mean ADC value; TIC, time intensity curve; TTP, time to peak; AUC, area under curve; Slope$_{max}$, maximum rise slope.					

FIGURE 1: Box-and-whisker plots show ADC (a), AUC (b), Slope$_{max}$ (c), and TTP (d) calculated for benign and malignant OLPDs group. The line in the box is the median, the height of the box represents interquartile range, whiskers are the lowest and highest data points still within the 1.5 interquartile range, and circles indicate outliers.

The flow void sign on T_2WI was the most significant qualitative conventional MRI feature that would be helpful in differentiating malignant OLPDs from benign mimics. This feature was found more frequently in benign OLPDs than in malignant mimics, which might be due to the hypervascular nature of benign OLPDs.[3] Besides that, the
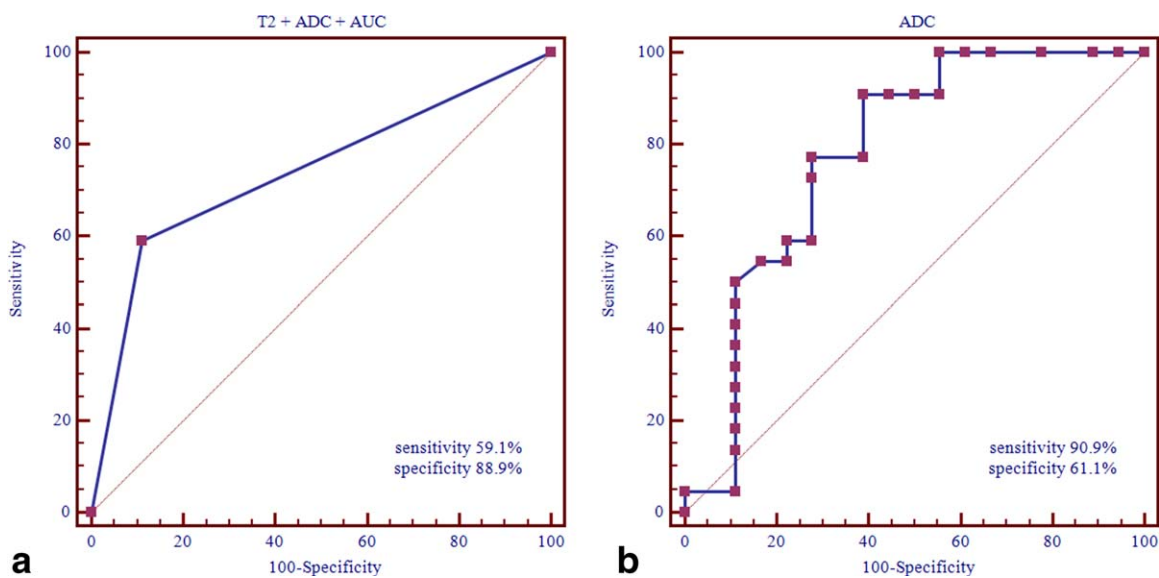

FIGURE 2: ROC curves of using T_2+ADC+AUC (a) and ADC (b) to differentiate orbital benign from malignant OLPDs. (a) Combination of "no presence of flow void sign on T_2WI" + ADC ≤0.886 × 10^{-3} mm^2/s + AUC ≤7.366 shows optimal specificity (88.9%), (b) while the ADC value alone shows optimal sensitivity (90.9%).

TABLE 5. Diagnostic Performance of Each Imaging Variable and Their Combinations

Model	Threshold value	AUC	Sensitivity	Specificity
T2WI	–	0.707 (0.542-0.840)	63.6% (40.7%-82.8%)	77.8% (52.4%-93.6%)
ADC	≤ 0.886	0.779 (0.620-0.895)	90.9%[a] (70.8%-98.9%)	61.1% (35.7%-82.7%)
AUC	≤ 7.366	0.795 (0.638-0.906)	77.3% (54.6%-92.2%)	72.2% (46.5%-90.3%)
T2WI+ADC	–	0.735 (0.572-0.862)	63.6% (40.7%-82.8%)	83.3% (58.6%-96.4%)
T2WI+AUC	–	0.712 (0.547-0.844)	59.1% (36.4%-79.3%)	83.3% (58.6%-96.4%)
ADC+AUC	–	0.758 (0.596-0.879)	68.2% (45.1%-86.1%)	83.3% (58.6%-96.4%)
T2WI+ADC+AUC	–	0.740 (0.577-0.865)	59.1% (36.4%-79.3%)	88.9%[b] (65.3%-98.6%)

ADC, apparent diffusion coefficient; AUC, area under curve; unit for ADC value is 10^{-3} mm^2/s. Data in parentheses is the 95% confidence interval.
[a]ADC value demonstrated highest sensitivity.
[b]Combination of T2, ADC, and AUC values demonstrated highest specificity.

patients with malignant OLPDs showed significantly older age than the patients with benign OLPDs in univariate analysis, which was similar to a prior study.[3] This result indicated that the patients' age should be considered in future clinical differentiation work. In addition, for the benign OLPDs, particularly the IgG4-related diseases, an extension of inflammatory changes to the mucosa of nasal and paranasal cavities could occur.[3] Therefore, benign OLPDs in our study showed more frequent imaging findings indicative of sinusitis than malignant mimics, which is similar to a prior study.[3] The imaging finding indicative of sinusitis also can provide potential supplemental
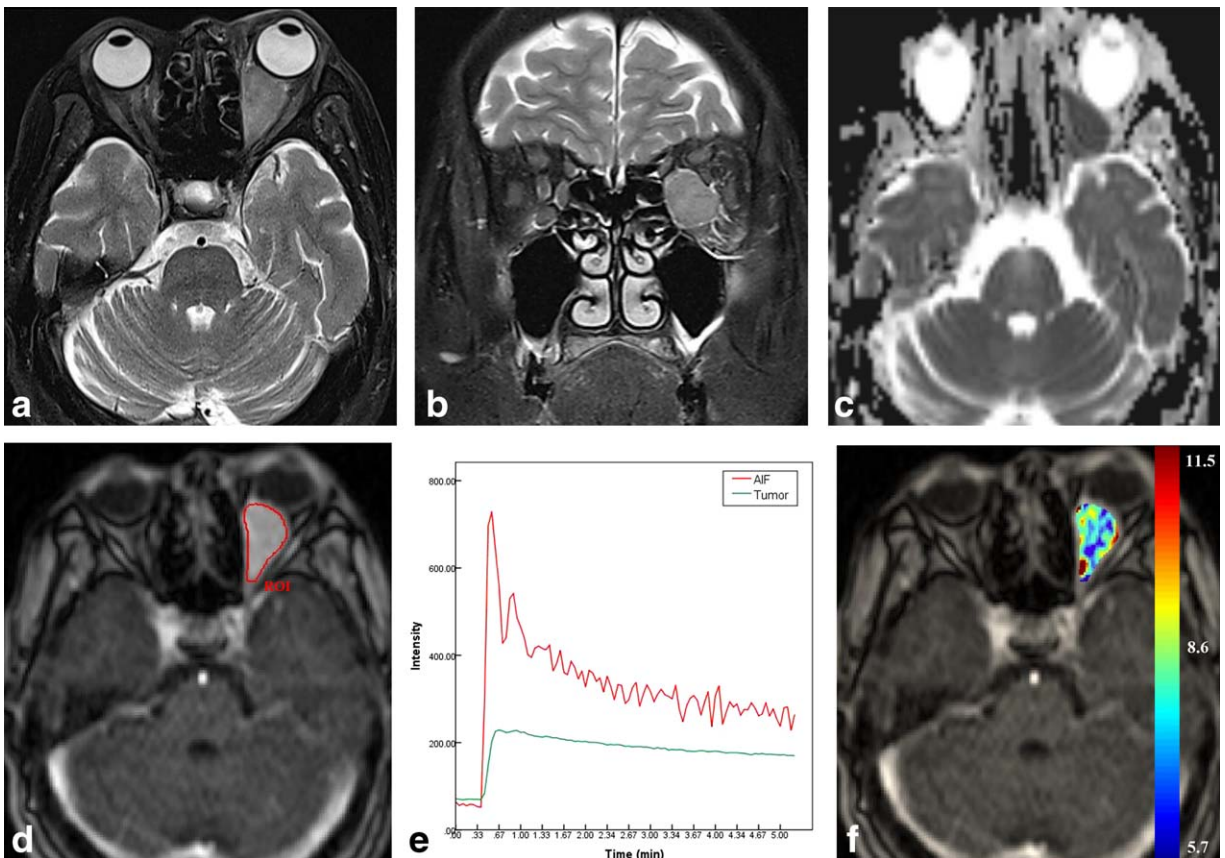

FIGURE 3: Mucosa-associated lymphoid tissue lymphoma in a 54-year-old man. (a) Axial and (b) coronal T_2WI show a mass located in the medial-inferior temporal quadrant of the left orbit. (c) The mass appears hypointense on the ADC map, the ADC value is 0.741 × 10^{-3} mm^2/s. (d) ROI drawn around the mass. (e) Obtained TIC shows as a washout pattern. (f) Color map for AUC is obtained, and the mean AUC value of this patient is 8.073.
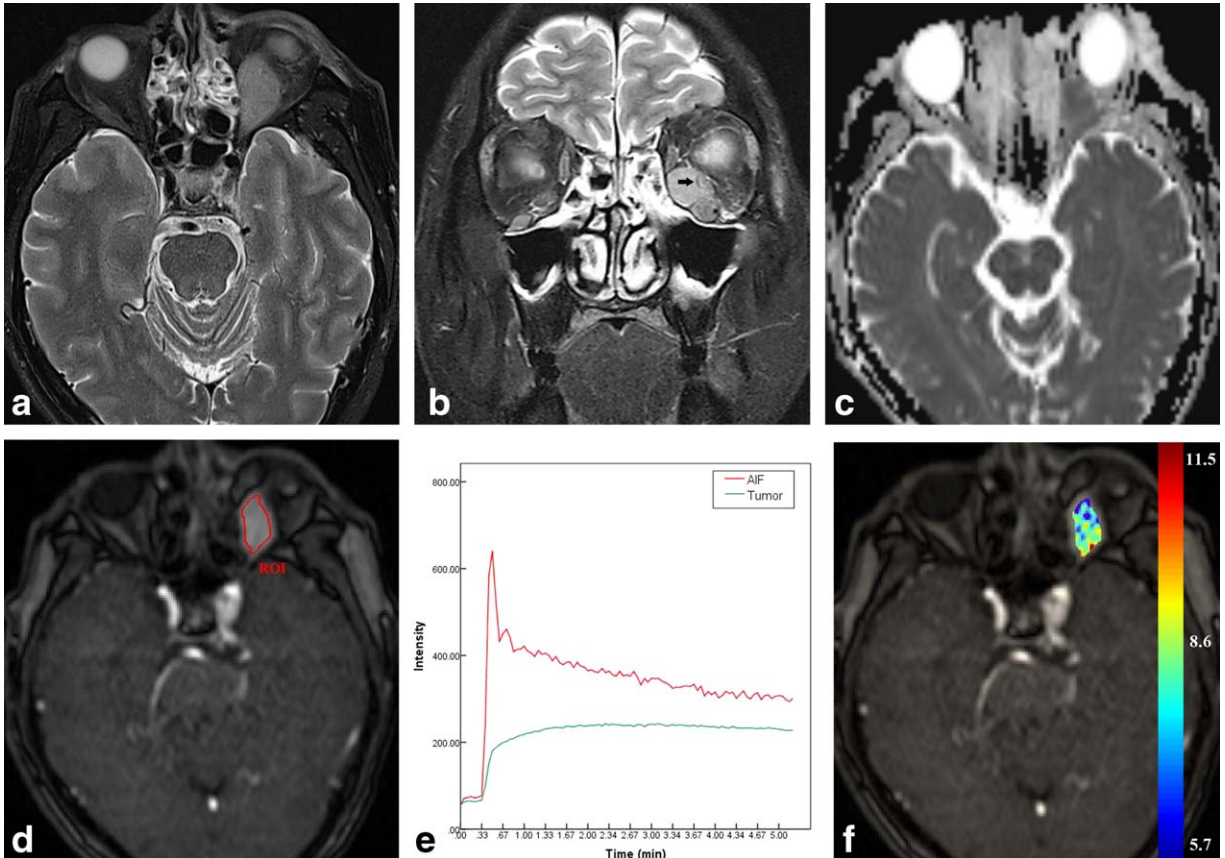
FIGURE 4: Idiopathic inflammatory pseudotumor in a 37-year-old man. (a) Axial T_2WI shows a mass located in the medial-inferior temporal quadrant of the left orbit. (b) Note the flow void signal (arrow) and the imaging findings suggestive of sinusitis on the coronal T_2WI. (c) ADC value of this mass is 1.003×10^{-3} mm^2/s. (d) ROI drawn around the mass. (e) Obtained TIC shows as a plateau pattern. (f) Color map for AUC is obtained, and the mean AUC value of this patient is 8.579.

information for differentiation work in clinical practice. Our study found no difference in tumor shape between the two groups, which differed from a prior study.[3] In our opinion, this contradiction might be due to the low reproducibility of qualitative MRI assessment, and this problem seems to be an important clinical obstacle.

In agreement with previous studies, we found that the mean ADC value of malignant OLPDs was significantly lower than that of the benign mimics.[3,6–12,22] This may be attributed to the enlarged nuclei and hypercellularity of the malignant OLPDs.[3,8,10] These typical histological characteristics may act to reduce the diffusion space in the extracellular and intracellular dimension with a resultant decrease in ADC value. Moreover, the interstitial changes in benign OLPDs would lead to an increased ADC value, which could also contribute to a difference in ADC value between benign and malignant OLPDs. Therefore, DWI and derived ADC values could serve as a promising imaging biomarker for differentiating benign and malignant OLPDs. However, the detailed ADC threshold value and diagnostic accuracy in the present study was not consistent with those of previous studies.[3,12] Haradome et al reported that an ADC value of less than 0.612×10^{-3} mm^2/s was optimal for diagnosing orbital lymphoma, while 0.886×10^{-3} mm^2/s was the opti-

mal threshold value in the present study.[3] The reasons for this discrepancy might be due to the variance in the pathological characteristics of the included lesions. Also, the magnetic field strength (1.5T or 3.0T) and b value (b = 800 or 1000 s/mm^2) would affect the ADC measurements.[3]

Unfortunately, the diagnostic specificity of DWI in our study was limited. This might be associated with the inclusion of IgG4-related orbital diseases in our study. IgG4-RD has been noted as a special benign OLPDs. It is also known as a dense lymphoplasmacytic infiltrate that is similar to lymphoma.[22] Restricted diffusion in IgG4-RD has been reported in the urethra and the pancreas.[23,24] The ADC value of orbital IgG4-RD in our study was also relatively lower than that of other benign OLPDs, and overlapped partially with that of the malignant OLPDs. The lower ADC values do not certainly indicate the diagnosis of malignant OLPDs, and IgG4-RD should also be considered, thus the diagnostic specificity would be influenced. Therefore, the differentiation work between orbital IgG4-RD and malignant OLPDs based on ADC measurement should be done carefully because of the potential overlap.

The application of DCE-MRI in the orbit has been reported with both 1.5T and 3.0T scanners.[5,14] Compared

with previous studies using a 1.5T MR scanner, higher temporal resolution could be achieved when a 3.0T MR scanner was used for DCE-MRI in the present study.[5,14] High temporal resolution is a critical component of high-quality DCE-MRI. It allows a more accurate assessment of the hemodynamic process as gadolinium contrast agent passes through the microvasculature in the tissue of interest.[16] The AUC parameter derived from DCE-MRI in benign OLPDs was significantly higher than that of the malignant OLPDs in the present study. The TIC pattern of these two entities could help us to explain this finding. In our study, the TIC pattern of benign OLPDs mostly showed as Type I (persistent pattern), while the malignant ones mostly showed as Type III (washout pattern), which was similar to a previous study.[14] Considering the similar TTP and Slope$_{max}$, naturally the AUC would demonstrate a significant difference between the two groups. However, despite that a significant difference was found, the AUC showed considerable overlap between the two entitles, and thus the diagnostic ability was limited, and further attempts to employ multiparametric MRI techniques are needed.

With the combination of conventional qualitative image assessment, DWI, and DCE-MRI techniques, optimal specificity could be achieved in differentiating benign from malignant OLPDs. In the clinical setting, the high specificity could be valuable in enhancing our diagnostic determination for potential malignancy, which is crucial for doctor–patient communication and determination of a therapy plan. However, the drawback of the combination of multiparametric MRI was the low sensitivity, which was unfavorable for identifying suspicious malignant OLPDs patients. By contrast, when using the ADC alone as the differentiating index, optimal sensitivity could be achieved. Therefore, we suggest using DWI as the filtering metric to identify patients with suspicious malignant OLPDs, and using the combination of conventional MR, DW, and DCE-MRI as the differentiating metric for diagnosing malignant OLPDs.

We acknowledge that this study has some limitations. First, it was a single-center retrospective study with a relatively small cohort, but we believe that our results are a strong basis for larger prospective studies. Second, the model-based parameters derived from DCE-MRI are preferable, as they provide greater insight about microvasculature physiology and tumor biology. A previous study pointed out that the calculation of model-based parameters showed poor reproducibility, which might be associated with the inter-reader variability in arterial input function measurement.[25] We chose model-free parameters because we wanted to minimize the dependence on complex pharmacokinetic modeling, and model-free parameters have also been proven to be robust indicators of tumor vascular characteristics.[26]

Despite the limitations, our study showed no presence of flow void sign on T_2WI as the most significant conventional MRI feature that might help to diagnose malignant OLPDs. The specificity of differentiating work could be significantly improved by adding DWI and DCE-MRI to conventional MRI alone. Meanwhile, DWI alone demonstrated the optimal sensitivity in differentiating orbital benign and malignant OLPDs.

REFERENCES

1. Tailor TD, Gupta D, Dalley RW, Keene CD, Anzai Y. Orbital neoplasms in adults: clinical, radiologic, and pathologic review. Radiographics 2013;33:1739–1758.

2. Priego G, Majos C, Climent F, Muntane A. Orbital lymphoma: imaging features and differential diagnosis. Insights Imaging 2012;3:337–344.

3. Haradome K, Haradome H, Usui Y, et al. Orbital lymphoproliferative disorders (OLPDs): value of MR imaging for differentiating orbital lymphoma from benign OPLDs. AJNR Am J Neuroradiol 2014;35:1976–1982.

4. Garner A. Orbital lymphoproliferative disorders. Br J Ophthalmol 1992;76:47–48.

5. Xian J, Zhang Z, Wang Z, et al. Value of MR imaging in the differentiation of benign and malignant orbital tumors in adults. Eur Radiol 2010;20:1692–1702.

6. Ben Simon GJ, Annunziata CC, Fink J, Villablanca P, McCann JD, Goldberg RA. Rethinking orbital imaging establishing guidelines for interpreting orbital imaging studies and evaluating their predictive value in patients with orbital tumors. Ophthalmology 2005;112:2196–2207.

7. Ro SR, Asbach P, Siebert E, Bertelmann E, Hamm B, Erb-Eigner K. Characterization of orbital masses by multiparametric MRI. Eur J Radiol 2016;85:324–336.

8. Xu XQ, Hu H, Su GY, et al. Orbital indeterminate lesions in adults: combined magnetic resonance morphometry and histogram analysis of apparent diffusion coefficient maps for predicting malignancy. Acad Radiol 2016;23:200–208.

9. Sepahdari AR, Kapur R, Aakalu VK, Villablanca JP, Mafee MF. Diffusion-weighted imaging of malignant ocular masses: initial results and directions for further study. AJNR Am J Neuroradiol 2012;33:314–319.

10. Xu XQ, Hu H, Su GY, et al. Utility of histogram analysis of ADC maps for differentiating orbital tumors. Diagn Interv Radiol 2016;22:161–167.

11. Razek AA, Elkhamary S, Mousa A. Differentiation between benign and malignant orbital tumors at 3-T diffusion MR imaging. Neuroradiology 2011;53:517–522.

12. Sepahdari AR, Aakalu VK, Setabutr P, Shiehmorteza M, Naheedy JH, Mafee MF. Indeterminate orbital masses: restricted diffusion at MR imaging with echo-planar diffusion-weighted imaging predicts malignancy. Radiology 2010;256:554–564.

13. Zhang Z, Shi J, Guo J, Yan F, Fu L, Xian J. Value of MR imaging in differentiation between solitary fibrous tumor and schwannoma in the orbit. AJNR Am J Neuroradiol 2013;34:1067–1071.

14. Yuan Y, Kuai XP, Chen XS, Tao XF. Assessment of dynamic contrast-enhanced magnetic resonance imaging in the differentiation of malignant from benign orbital masses. Eur J Radiol 2013;82:1506–1511.

15. Carmeliet P, Jain RK. Angiogenesis in cancer and other diseases. Nature 2000;407:249–257.

16. Gaddikeri S, Gaddikeri RS, Tailor T, Anzai Y. Dynamic contrast-enhanced MR imaging in head and neck cancer: techniques and clinical applications. AJNR Am J Neuroradiol 2016;37:588–595.

17. Yuan M, Zhang YD, Zhu C, et al. Comparison of intravoxel incoherent motion diffusion-weighted MR imaging with dynamic contrast-enhanced MRI for differentiating lung cancer from benign solitary pulmonary lesions. J Magn Reson Imaging 2016;43:669–679.

18. Huang B, Wong CS, Whitcher B, et al. Dynamic contrast-enhanced magnetic resonance imaging for characterising nasopharyngeal carcinoma: comparison of semiquantitative and quantitative parameters and correlation with tumour stage. Eur Radiol 2013;23:1495–1502.

19. Jia ZZ, Gu HM, Zhou XJ, et al. The assessment of immature microvascular density in brain gliomas with dynamic contrast-enhanced magnetic resonance imaging. Eur J Radiol 2015;84:1805–1809.

20. Dutoit JC, Claus E, Offner F, Noens L, Delanghe J, Verstraete KL. Combined evaluation of conventional MRI, dynamic contrast-enhanced MRI and diffusion weighted imaging for response evaluation of patients with multiple myeloma. Eur J Radiol 2016;85:373–382.

21. Wu CJ, Wang Q, Li H, et al. DWI-associated entire-tumor histogram analysis for the differentiation of low-grade prostate cancer from intermediate-high-grade prostate cancer. Abdom Imaging 2015;40:3214–3221.

22. Hiwatashi A, Yoshiura T, Togao O, et al. Diffusivity of intraorbital lymphoma vs. IgG4-related disease: 3D turbo field echo with diffusion-sensitised driven-equilibrium preparation technique. Eur Radiol 2014;24:581–586.

23. Choi JW, Kim SY, Moon KC, Cho JY, Kim SH. Immunoglobulin G4-related sclerosing disease involving the urethra: case report. Korean J Radiol 2012;13:803–807.

24. Taniguchi T, Kobayashi H, Nishikawa K, et al. Diffusion-weighted magnetic resonance imaging in autoimmune pancreatitis. Jpn J Radiol 2009;27:138–142.

25. Koh MJ, Kim HS, Choi CG, Kim SJ. Which is the best advanced MR imaging protocol for predicting recurrent metastatic brain tumor following gamma-knife radiosurgery: focused on perfusion method. Neuroradiology 2015;57:367–376.

26. Boxerman JL, Schmainda KM, Weisskoff RM. Relative cerebral blood volume maps corrected for contrast agent extravasation significantly correlate with glioma tumor grade, whereas uncorrected maps do not. AJNR Am J Neuroradiol 2006;27:859–867.